High-Performance Flow Simulation and Scale-Adaptive Turbulence Modelling of Centrifugal Pumps

M. Hundshagen, N. Casimir, A. Pesch, R. Skoda

published in

NIC Symposium 2020

M. Müller, K. Binder, A. Trautmann (Editors)

Forschungszentrum Jülich GmbH, John von Neumann Institute for Computing (NIC), Schriften des Forschungszentrums Jülich, NIC Series, Vol. 50, ISBN 978-3-95806-443-0, pp. 367. http://hdl.handle.net/2128/24435

© 2020 by Forschungszentrum Jülich

Permission to make digital or hard copies of portions of this work for personal or classroom use is granted provided that the copies are not made or distributed for profit or commercial advantage and that copies bear this notice and the full citation on the first page. To copy otherwise requires prior specific permission by the publisher mentioned above.

High-Performance Flow Simulation and Scale-Adaptive Turbulence Modelling of Centrifugal Pumps

Markus Hundshagen, Nicolas Casimir, Andreas Pesch, and Romuald Skoda

Chair of Hydraulic Fluid Machinery, Ruhr University Bochum, 44801 Bochum, Germany E-mail: romuald.skoda@ruhr-uni-bochum.de

While for the design point operation of centrifugal pumps, where an essentially steady flow field is present and statistical turbulence models yield an appropriate prediction of the characteristics, the flow field gets increasingly unsteady towards off-design operation. Special designs as e. g. sewage pumps are characterised by a single-blade impeller and show significantly unsteady characteristics even in the design point. For such highly-unsteady and turbulent flow fields, statistical models tend to fail. On the other hand, Large-Eddy Simulation models, where the largevortex part of the turbulent spectrum is directly resolved, show a much better flow prediction. However, the spatial resolution and thus computational effort are too high for engineering real pump applications. Therefore, we provide an assessment of scale-adaptive turbulence simulation (SAS) models that recover a statistical flow solution in regions of low unsteadiness and like Large-Eddy Simulation - resolve a part of the turbulent spectrum down to the available grid resolution for highly unsteady flow regions. After a thorough validation on standard turbulence test cases e. g. the periodic hill case, it is shown that with a moderately higher computational effort than statistical models, the SAS yields a considerable improvement of the prediction of the turbulence field in part load operation of a centrifugal pump while the mean flow field could be well predicted even with a well-established statistical model.

1 Introduction

Increasing demands on centrifugal pumps, e. g. by legislature, require higher efficiencies even at off-design operation, i. e. part load and overload, which are characterised by a highly unsteady and turbulent flow field due to flow separation and impeller-stator interaction. CFD methods are increasingly integrated in the design and optimisation process of pumps. Statistical (i. e. URANS) eddy-viscosity turbulence models are widely used for pump flow simulations. In this class of turbulence models, a significant simplification is introduced by an a priori time-average of the turbulent fluctuations. Thus, the resulting Reynolds-stress tensor has lost any spectral information of the turbulence field. Although statistical models may yield a good prediction of pump characteristics at closeto-design operation, they may increasingly fail towards off-design pump operation. In a previous study, a comparison of spatially and temporally high resolved measurement data to URANS simulations with the k- ω -Shear Stress Transport (SST) turbulence model¹ (referred to as SST in what follows) revealed that, although time-averaged head and ensembleaveraged flow angle were in good agreement for design and part load operation, turbulence intensity (TI) is over-predicted especially in part load operation near the volute tongue.² There are several other studies that show limitations of statistical models and benefits of scale-resolving Large-Eddy Simulation models (LES).^{3–12} However, the computational effort of LES is tremendous at high Reynolds numbers encountered in centrifugal pumps because at least 80 % of the spectral energy must be resolved 13, 14 and a soundly resolved LES demands therefore an extensively high number of computational cells and very small

time steps. In most LES studies on centrifugal pumps, it remains unclear if a sufficient amount of the spectral energy is resolved to fulfil the LES criteria.

An interesting approach is the Scale-Adaptive Simulation method, ¹⁵ which is an improvement of statistical models with the ability to resolve the turbulent spectrum down to the available grid limit. This is achieved by a reduction of turbulent viscosity depending on the von Karman length scale and the integral length scale. A variant of this model is the $k-\omega$ -SST-SAS model (referred to as SAS). ¹⁶ Especially the fall-back of the SAS to a SST solution in regions of low spatial and temporal resolution is a convenient way to avoid uncertainties in spectral energy resolution. ¹⁶ Several studies show the improvement of prediction accuracy of this type of model in highly transient flow compared to statistical turbulence models. ^{5, 8, 12, 17, 18} However, in these studies it remains unclear what the "critical" spatial grid resolution is to activate the scale-resolving capability of SAS and thus to achieve an improvement over SST solutions. Therefore, we want to assess the capability of the SAS model with focus on grid dependence for centrifugal pump flow.

2 Numerical Method and Validation

The incompressible Navier-Stokes equations in their unsteady Reynolds-averaged form (URANS) are solved by the open source software foam-extend version 4.0.^a The software foam-extend is a C++ toolbox for the development of customised solvers. A conservative finite volume co-located unstructured spatial discretisation is chosen. We utilise central differences in combination with second order total variation diminishing (TVD) differencing schemes for convective fluxes for scale resolving turbulence models. An implicit pressure based solver is utilised, i. e. a combined PISO¹⁹ and SIMPLE²⁰ algorithm for incompressible unsteady flows since it is the most efficient choice for relatively small time steps with a Courant number ~ 1 . We combine this solver with moving mesh capabilities. For the evaluation of convergence of the non-linear iterative PISO-SIMPLE algorithm, preliminary investigations have shown that a drop of the non-linear non-dimensional residual sum norm of each equation below a value of 10^{-5} is a suitable convergence criterion. While the statistical two-equation eddy-viscosity SST turbulence model by Menter¹ has been already available in the standard package of the software, we have implemented an SAS extension by Menter. 16 The statistical (SST) and scale-adaptive (SAS) variant only deviate by an additional source term in the dissipation scale (ω) equation so that the computational effort is essentially the same if the temporal and spatial resolution is the same.

To show the performance of the SAS, we have investigated several standard test cases that have been optimised for turbulence model assessment. *E. g.* in the channel and duct flow as well as asymmetric diffusor case (not shown here) the SAS model is not able to switch from URANS to scale-resolving simulations without an explicit introduction of synthetic turbulence and thus falls back to the statistical SST solution as has been observed also in other studies, *e. g.* Mehdizadeh *et al.*²¹ Thus, we focus on the "periodic hill" test case where the periodic in- and outflow conditions support an amplification of model inaccuracies and is thus particularly challenging for turbulence models. In fact, the statistical SST variant completely fails to predict the separation and re-attachment location of the pronounced separation downstream of the hills (not shown here). On the other hand, we

ahttp://foam-extend.fsb.hr/

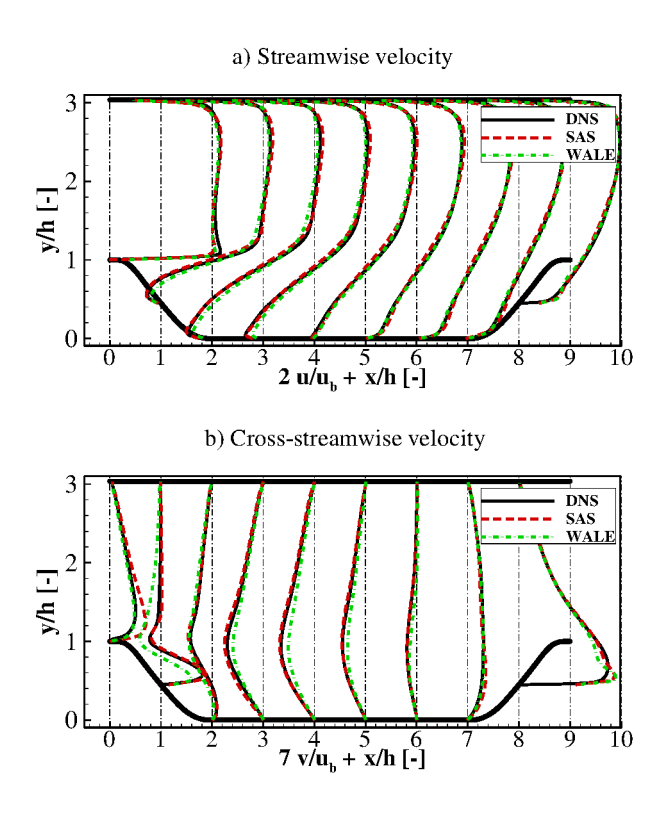


Figure 1. Mean velocity field of the periodic hill test case at bulk Reynolds number $Re_b = 10.595$. DNS data by Krank $et\ al.^{23}$

observe a distinct scale-resolving mode of the SAS model. In Fig. 1 a comparison of the SAS and a classical LES solution by the WALE model²² is provided. We have performed the simulations on different computational grid resolutions (one simulation run on the finest grid demands an effort of about 60 thousand core hours) and show only the coarsest grid solution here to demonstrate the SAS model performance with "engineering" resources in terms of relatively coarse grids. In addition, benchmark data from Direct Numerical Simulations (DNS) by Krank et al.²³ are included in Fig. 1. The SAS matches the benchmark data and thus provides an essential improvement to the statistical SST solution. While for the stream-wise velocity component, c.f. Fig. 1(a), neither significant differences between SAS and LES nor between the grids (not shown) are discernible, it is interesting to see that for the cross-stream-wise component, c.f. Fig. 1(b), the LES for the coarser grid shows a significant deviation from data that diminishes with grid refinement (not shown here). The SAS solution matches the data well even on the coarse grid. Thus, this exemplary observation underlines the benefit of the SAS to yield appropriate results even on grids that do not fulfil the tremendous spatial and temporal resolution demands of a LES and where the LES may yield inaccurate results due to an under-resolution of the spectral energy cascade. This observation will be further explored in a centrifugal pump in what follows.

3 Centrifugal Pump Test Case

A single stage volute casing radial centrifugal pump (specific speed $n_S = 26 \text{ min}^{-1}$) is investigated at part load operation. The pump is operated with air in order to enable hotwire anemometry measurements for a high temporal and spatial resolution of the velocity field near the impeller discharge (measurement plane depicted in Fig. 2(b)) and thus enables a comparison with turbulence statistics from the simulation. Since the maximum Mach number is evaluated to be below 0.3, it is assumed that compressibility effects on the velocity field are of minor relevance. Pump details and experimental data are documented by Hergt *et al.*, ²⁴ Meschkat and Stoffel²⁵ and Casimir *et al.*² and are briefly summarised here.

The head characteristics is discussed by Casimir $et\ al.$, where a good agreement between measurement and simulation has been obtained even with the statistical SST model. However, deviations of the local turbulence field in part load could be observed. Thus in the present study, we focus our attention to a discussion of the local velocity field and not on the integral characteristics. Mean flow angle and standard deviation of velocity (RMS) are presented in the measurement plane as functions of the axial position y/b, c.f. Fig. 2(a), the circumferential coordinate ε , c.f. Fig. 2(b) and the time coordinate x/t, which corresponds to the time range when one blade spacing passes the measurement position, c.f. Fig. 2(c). The local flow-angle α is evaluated with Eq. 1

$$\alpha = \frac{|c_{\rm r}|}{c_{\rm r}}a\cos\left(\frac{c_{\rm u}}{c_{\rm abs}}\right) \tag{1}$$

where c_r is the radial velocity component, $c_{\rm u}$ is the circumferential velocity component and $c_{\rm abs}$ is the magnitude of the absolute velocity. $\alpha < 90^\circ$ means backflow and $\alpha > 90^\circ$ means outflow against the rotational direction. Measured TI is evaluated by the RMS of the absolute velocity magnitude according to Eq. 2 and includes turbulent as well as non-

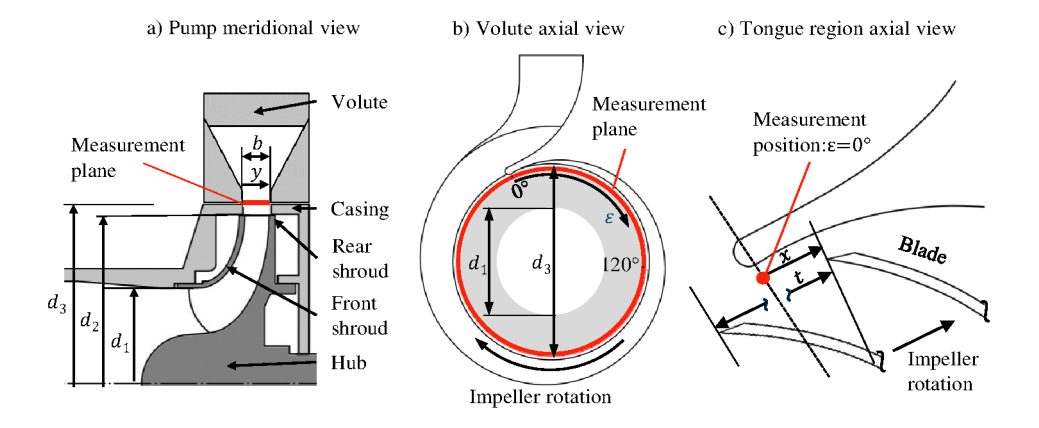


Figure 2. (a) Meridional contour; (b) Measurement plane; (c) Illustration of coordinate x, which corresponds to the time range when one blade spacing passes the measurement position.

turbulent fluctuations.

$$TI_{EXP} = \frac{RMS(c_{abs})}{u_2} \tag{2}$$

 u_2 is the circumferential impeller trailing edge velocity. For the simulations, a TI comparable to measurements is evaluated by taking into account temporally resolved URANS-velocity fluctuations (Eq. 3) and ensemble-averaged turbulent kinetic energy \overline{k} (Eq. 4):

$$TI_{RMS} = \frac{\sqrt{RMS^2(c_{abs,Sim})}}{u_2}$$
 (3)

$$TI_{TKE} = \frac{\sqrt{2\bar{k}_{Sim}}}{u_2} \tag{4}$$

k corresponds to a priori time-averaged fluctuation in the URANS approach. Thus, total TI is evaluated according to Eq. 5 in the simulation.

$$TI_{SIM} = \frac{\sqrt{(RMS^2(c_{abs,Sim}) + 2\overline{k}_{Sim})}}{u_2}$$
 (5)

For further information on the evaluation methods, we refer to Casimir *et al.*² and Pesch *et al.*²⁶

4 Numerical Setup

The computational domain contains the impeller, volute casing, side chambers and the suction and pressure pipe, c.f. Fig. 3(c). The suction pipe has been elongated to a length of $5 \times D$ to avoid an impact of boundary conditions on the part load vortex. A block structured hexahedral grid as shown in Fig. 3(b) with approximately 3 million nodes (named G1) is generated. For a grid study, the grid G1 is successively refined to approximately 24 million nodes (named G2) by bisection of node distances in each direction. For G1, average and maximum y^+ values equal about 10 and 60, and for G2 about 5 and 30, respectively. The fluid is incompressible air with a kinematic viscosity of $\nu=10^{-5} \mathrm{m}^2/\mathrm{s}$.

A Dirichlet inlet boundary condition is set for velocity according to flow rates from experiment, together with a Neumann (zero-gradient) condition for static pressure. At the volute discharge, a Neumann boundary conditions is set for velocity (zero gradient) and a Dirichlet condition for static pressure. Temporal and spatial second order discretisation methods are used. Tabs. 1 and 2 list the settings for SST and for SAS simulations, respectively. As the time step size needs to be small with the SAS model (CFL $_{\rm max}$ < 1), the solver is run in PISO mode, *i. e.* only one outer corrector step is performed for SAS simulations.

The rotating domain includes the suction pipe, impeller and side chambers, and the stationary domain includes the volute-casing and discharge pipe, *c.f.* Fig. 3(c). The governing equations are solved in the absolute frame of reference so that a moving grid is applied for the rotating domain. Thus, the rotor and the stator grid need to be coupled at each time step. Transient coupling of rotor and stator domain is achieved by a General Grid Interface (GGI) algorithm by Beaudoin and Jasak³⁰ that allows a non-conformal grid, *i. e.* non-matching grid nodes on both, rotor and stator side of the interface. As described by

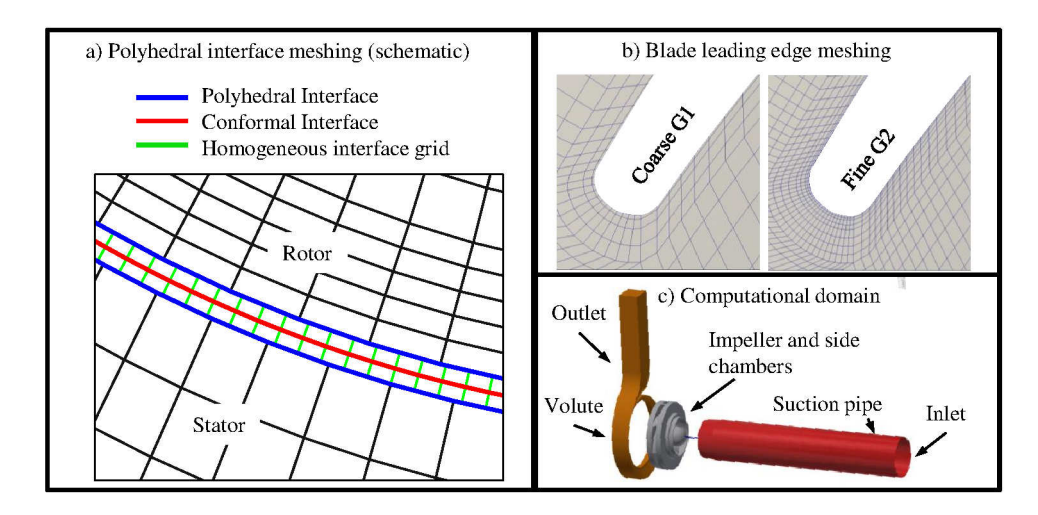


Figure 3. (a) Schematic illustration of the rotor-stator interface grid; (b) Computational grid at the blade leading edge; (c) Computational domain.

Casimir $et\ al.^2$ and Pesch $et\ al.^{26}$ the algorithm yields spurious oscillations for non-planar interfaces due to local non-conservative flux transmission and thus needs to be modified for the impeller-stator sliding interface. We introduced a polyhedral interface meshing, c.f. Fig. 3(a) and a thin homogeneous interface grid whose circumferential node distribution matches the circumferential rotor movement within each time step, yielding matching interface nodes and thus a conservative interface at each time step, referred to as conformal interface. Details on the rotor-stator interface can be found in Casimir $et\ al.^2$ and Pesch $et\ al.^{26}$

Parameter	Description
Turbulence model	SST ¹
Wall functions	k: kqrWallFunction ν_t : nutWall-Function ω : omegaWallFunction
Time discretisation	Backward Euler
Discretisation (div U)	LinearUpwind ²⁷
Discretisation (k and ω)	vanLeer ²⁸
Linear solver for p	BiCGStab
Linear solver (U, k, ω)	smoothSolver
Time step size	$1 \circ \rightarrow \text{CFL} \approx 30$
nCorrectors (PISO loops)	2
nOuterCorrectors (PIMPLE loops)	max. 50 with convergence control

Table 1. Summary of the numerical setup for SST simulations.

Parameter	Description
Turbulence model	SAS ¹⁶
Wall functions	see Tab. 1
Time discretisation	Backward Euler
Discretisation (div U)	DESHybrid ²⁹
Discretisation (k and ω)	vanLeer ²⁸
Linear solver for p	BiCGStab
Linear solver for U, k, ω	smoothSolver
Time step size	$1/32$ ° \rightarrow CFL < 1
nCorrectors (PISO loops)	2
nOuterCorrectors (PIMPLE loops)	1

Table 2. Summary of the numerical setup for SAS simulations.

For implicit pressure based solvers, a large part of the computational resources in terms of CPU-time are utilised for solving the pressure equation. Preconditioned conjugated gradient solvers (PCG) for the solution of the linear equation system have been found to be most efficient. The re-calculation of the flux assignments at the rotor-stator interface after each mesh motion step also contributes considerably to the resources. The code is parallelised with OpenMPI. For the benchmark, SAS simulations on a grid of 24 million cells with up to 20 computational nodes (960 Cores) are performed on the JUWELS cluster. A constant number of pressure iterations per time step is specified for the scaling assessment. A total amount of 4 time steps is calculated and one write operation of the solution is considered for the benchmark. The resulting scaling characteristics are shown in Fig. 4. It is noticeable, that the scaling behaviour is nearly ideal up to 12 nodes (42 000 cells per core), which is mainly related to the excellent scalability of the PCG solver. The used amount of memory per node is approximately 16 GB.

Regarding data storage, large write operations are done for full-3D backup results with a size of \sim 5 GB and a temporal interval of 5 minutes on 960 cores, while more frequent write operations are performed for monitoring results every 4 seconds with \sim 20 MB of data.

5 Results

Ensemble-averaged mean flow angle α and TI are evaluated in the measurement plane in the impeller wake and compared between measurement and simulation for part load, *i. e.* at 40 % of the nominal pump load. In this off-design operation, turbulent flow unsteadiness is highly distinctive. Statistical convergence of the measurements is achieved by an ensemble-average over more than 100 impeller revolutions. For ensemble-averaging, 7 values per revolution are available for the 7-blade impeller. For SAS simulations, less revolutions are considered for ensemble-averaging due to the limit of computational resources, what results in a significantly smaller amount of samples than for the measurements.

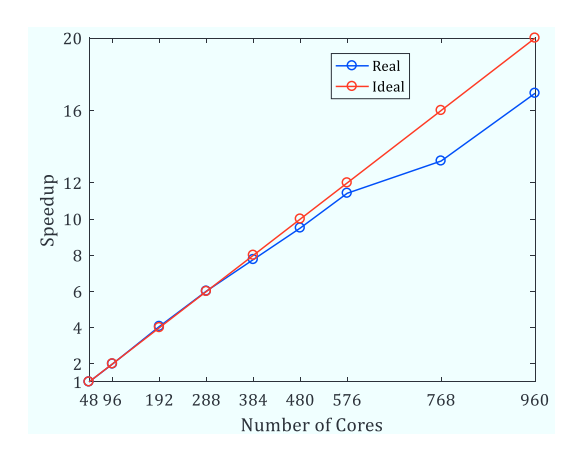


Figure 4. Scaling characteristics on JUWELS with a problem size of 24 million cells.

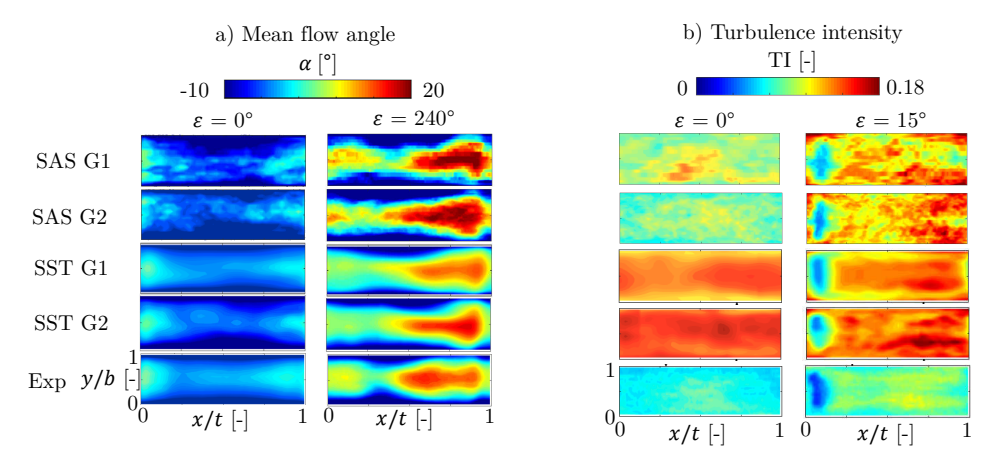


Figure 5. Ensemble-average flow angle (a) and turbulence intensity (b) for different circumferential volute positions ε .

Fig. 5(a) shows a comparison of an ensemble-averaged flow angle between SST, SAS and measurement data for two different volute positions near $\varepsilon=0^\circ$ and far off the volute tongue at $\varepsilon=240^\circ$. A noisy appearance of the contour plots shows that statistical convergence has not been achieved completely yet for the SAS simulations. Nevertheless, since preliminary evaluations of different numbers of ensembles did not show a significant change of the relevant pattern, a sufficiently reliable assessment of the SAS flow angle in comparison to both SST results and measurement data is assumed to be feasible. No significant mesh dependence is observed for the flow angle. The flow at the volute tongue at $\varepsilon=0^\circ$ is dominated by an outflow around the blade trailing edge (near x/t=0 and x/t=1) and a secondary back flow near the sidewalls (y/b=0 and y/b=1) at mid-channel (x/t=0.5). This behaviour can be seen on both grids for SAS and SST. Thus, SAS and SST results can be considered equally close to measured flow angle in terms of spatially resolved and ensemble-averaged flow angle.

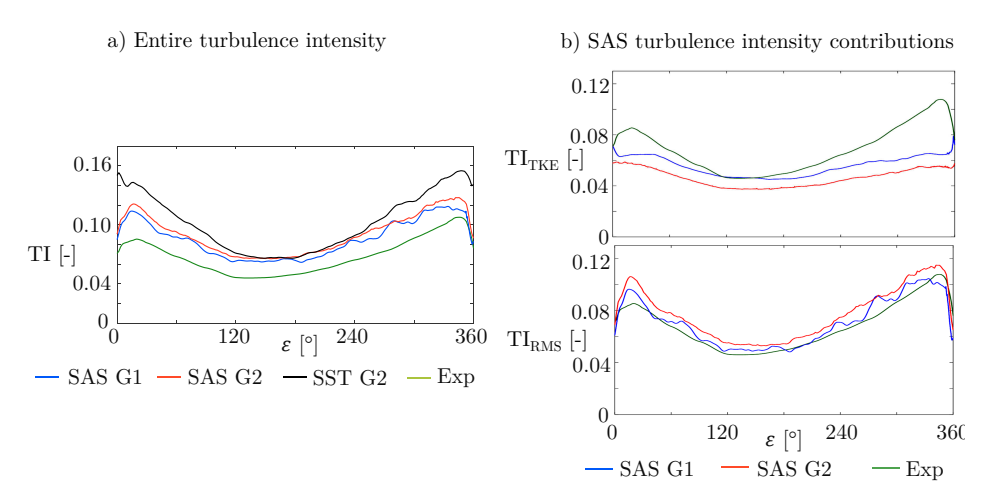


Figure 6. Axially and time-averaged TI for simulation and measurement data (a) and contributions to TI for the SAS model (b).

Regarding the TI results, for the SST model a significant overestimation can be seen in the immediate vicinity of the volute tongue at $\varepsilon=0^\circ$ (c. f. Fig. 5(b), left column) that gets even more pronounced with grid refinement. The TI is reduced significantly with the SAS model and thus matches the experimental data much better, particularly for the finer grid G2, what is a distinctive improvement of TI prediction. In the other volute regions in circumferential direction, here represented by the $\varepsilon=15^\circ$ position, TI is over-predicted systematically by both models.

Fig. 6(a) shows the axially and time-averaged TI distribution vs. circumferential volute position ε , where this behaviour is reflected over the entire spectrum of ε . In Fig. 6(a) TI for the simulation has been evaluated by Eq. 2. In order to provide a more comprehensive illustration of TI by the SAS model, Fig. 6(b) shows the two contributions to TI according to Eqs. 3 and 4. The amount of TI_{RMS} is higher for G2 which shows the scale-adaptive behaviour of the model, as with grid refinement the amount of resolved turbulent fluctuations increases. TI_{TKE} is lower for grid G2. Interestingly, the discrepancy of total TI to measurement data cannot be reduced by grid refinement. We assume that, since G1 and G2 are still in the range of wall functions, this may be a consequence of the impeller wake flow, and a wall-adjacent grid refinement towards low-Reynolds wall treatment in the impeller may improve the results, which will be the subject of further investigations.

6 Conclusions

Deviations of the ensemble-averaged flow angle to measurement data are small for both turbulence models, so that the SST model is found to be sufficiently accurate for mean flow prediction, *e. g.* mean flow angle. A different conclusion can be drawn for turbulent quantities, such as TI. A significant improvement of TI prediction near the volute tongue is found for the SAS model compared to SST results. Afar from the volute tongue, total TI is overestimated with both turbulence models. In particular the fact that a grid refinement

does not reduce the entire TI level (TI_{RMS} and TI_{TKE}) for the SAS model will be the subject of further studies.

The results presented on the 7 blade specific speed $n_S=26~min^{-1}$ pump are an extract of our pump simulation efforts and are representative of our turbulence modelling approach. A highly unsteady flow field that demands accurate turbulence predictions is also present in extremely low specific speed pumps ($n_S<12~min^{-1}$) and special designs, such as single-blade pumps or positive displacement pumps. The findings presented here will also be transferred to these pump types.

Although we could show that the SAS model in its present form shows an improvement over the SST model even on a moderate grid resolution, a further improvement to obtain also a quantitative agreement to measurement data will be done in further studies by a thorough exemplary assessment *vs.* reference simulation data in terms of well-resolved LES results.

Acknowledgements

The authors gratefully acknowledge the Gauss Centre for Supercomputing e.V. (www.gauss-centre.eu) for providing computing time through the John von Neumann Institute for Computing (NIC) on the GCS Supercomputers JURECA and JUWELS at Jülich Supercomputing Centre (JSC). The authors also gratefully acknowledge the financial support by the "Forschungskuratorium Maschinenbau e.V.". This project is funded by the Federal Ministry for Economic Affairs (BMWi).

References

- 1. F. R. Menter, M. Kuntz, and R. Langtry, *Ten Years of Industrial Experience with the SST Turbulence Model*, in Proceedings of the 4th International Symposium on Turbulence, Heat and Mass Transfer, Begell House, 625–632, 2003.
- N. Casimir, Z. Xiangyuan, G. Ludwig, and R. Skoda, Assessment of statistical eddyviscosity turbulence models for unsteady flow at part and overload operation of centrifugal pumps, in Proceedings of 13th European Conference on Turbomachinery Fluid dynamics & Thermodynamics (ETC13), Lausanne, ETC2019-047, 2019.
- 3. R. K. Byskov, C. B. Jacobsen, and N. Pedersen, *Flow in a Centrifugal Pump Impeller at Design and Off-Design Conditions Part II: Large Eddy Simulations*, Journal of Fluids Engineering **125**, 73–83, 2003.
- 4. C. Kato, H. Mukai, and A. Manabe, *Large-Eddy Simulation of Unsteady Flow in a Mixed-Flow Pump*, International Journal of Rotating Machinery **9**, 345–351, 2003.
- 5. A. Posa, A. Lippolis, and E. Balaras, *Large-eddy simulation of a mixed-flow pump at off-design conditions*, Journal of Fluids Engineering **137**, 2015.
- A. Posa, A. Lippolis, R. Verzicco, and E. Balaras, Large-eddy simulations in mixedflow pumps using an immersed-boundary method, Computers & Fluids 47, 33–43, 2011.
- 7. J. Shen, Y. Li, Z. Liu, and X. Tang, *Turbulent flow and pressure fluctuation prediction of the impeller in an axial-flow pump based on LES*, 6th Int. Conf. on Pumps and Fans with Compressors and Wind Turbines; IOP Conference Series: Material Science and Engineering **52**, 032015, 2013.

- 8. Q. Si, J. Yuan, S. Yuan, W. Wang, L. Zhu, and G. Bois, *Numerical Investigation of Pressure Fluctuation in Centrifugal Pump Volute Based on SAS Model and Experimental Validation*, Advances in Mechanical Engineering **6**, 972081, 2014.
- 9. T. Tokay and S. Constantinescu, *Validation of a large eddy simulation model to simulate flow in pump intakes of realistic geometry*, Journal of Hydraulic Engineering **132**, 1303–1315, 2006.
- 10. W. Wang and Y. Wang, *Analysis of inner flow in low specific speed centrifugal pump based on LES*, Journal of Mechanical Science and Technology **27**, 1619–1626, 2013.
- 11. Y. Wu, X. Tang, F. Wang, An improved large eddy simulation of two-phase flows in a pump impeller, Acta Mech. Sin. 23, 635, 2007.
- 12. W. Zhang, Y. Yu, and H. Chen, *Numerical Simulation of Unsteady Flow in Centrifugal Pump Impeller at Off-Design Condition by Hybrid RANS/LES Approaches*, in High Performance Computing and Applications, Lecture Notes in Computer Science **5938**, Springer, 571–578, 2010.
- 13. J. Fröhlich, *Large Eddy Simulation turbulenter Strömungen: mit 14 Tabellen*, Lehrbuch Maschinenbau, Teubner, Wiesbaden, 1. Edition, 2006.
- 14. S. B. Pope, *Turbulent Flows*, Cambridge University Press, 2000.
- 15. J. C. Rotta, *Turbulente Strömungen: eine Einführung in die Theorie und ihre Anwendung*, B. G. Teubner, Stuttgart, 1972.
- F. R. Menter and Y. Egorov, The Scale-Adaptive Simulation Method for Unsteady Turbulent Flow Predictions. Part 1: Theory and Model Description, Flow, Turbulence and Combustion 85, 113–138, 2010.
- 17. A. Lucius and G. Brenner, *Unsteady CFD simulations of a pump in part load conditions using scale-adaptive simulation*, International Journal of Heat and Fluid Flow **31**, 1113–1118, 2010.
- J. Schiffer, C. Bodner, H. Jaberg, S. Korupp, and L. Runte, *Performance analysis of a single-blade impeller pump based on unsteady 3D numerical simulation*, in Proceedings of the 3rd International Rotating Equipment Conference, Düsseldorf, 193–203, 2016.
- 19. R. I. Issa, Solution of the implicitly discretised fluid flow equations by operator-splitting, Journal of Computational Physics **62**, 40–65, 1986.
- 20. S. V. Patankar and D. B. Spalding, *A calculation procedure for heat, mass and momentum transfer in three-dimensional parabolic flows*, in Numerical Prediction of Flow, Heat Transfer, Turbulence and Combustion, Elsevier, 54–73, 1983.
- 21. A. Mehdizadeh, H. Foroutan, G. Vijayakumar, and A. Sadiki, *A new formulation of scale-adaptive simulation approach to predict complex wall-bounded shear flows*, Journal of Turbulence **15**, 629–649, 2014.
- 22. F. Nicoud and F. Ducros, *Subgrid-Scale Stress Modelling Based on the Square of the Velocity Gradient Tensor*, Flow, Turbulence and Combustion **62**, 183–200, 1999.
- 23. B. Krank, M. Kronbichler, and W. A. Wall, *Direct Numerical Simulation of Flow over Periodic Hills up to Re*_H = 10,595, Flow, Turbulence and Combustion **101**, 521–551, 2018.
- 24. P. Hergt, S. Meschkat, and B. Stoffel, *The flow and head distribution within the volute of a centrifugal pump in comparison with the characteristics of the impeller without casing*, Journal of Computational and Applied Mechanics **5**, 275–285, 2004.

- 25. S. Meschkat and B. Stoffel, *The local specific head at different circumferential positions in a volute casing centrifugal pump in comparison to the characteristic curve of the single rotor*, in Proceedings of the Hydraulic Machinery Systems 21st IAHR Symposium, Lausanne, 2002.
- 26. A. Pesch, N. Casimir, M. Hundshagen, and R. Skoda, *Assessment of Scale Adaptive Turbulence Modeling in Centrifugal Pump Simulations*, 14th OpenFOAM Workshop, Duisburg, 2019.
- 27. R. F. Warming and R. M. Beam, *Upwind Second-Order Difference Schemes and Applications in Aerodynamic Flows*, AIAA Journal **14**, 1241, 1976.
- 28. B. Van Leer, *Towards the Ultimate Conservative Difference Scheme. V. A Second-Order Sequel to Godunov's Method*, Journal of Computational Physics **32**, 101–136, 1979.
- 29. M. Strelets, *Detached eddy simulation of massively separated flows*, in 39th Aerospace Sciences Meeting and Exhibit, 2001.
- 30. M. Beaudoin and H. Jasak, *Development of a Generalized Grid Mesh Interface for Turbomachinery simulations with OpenFOAM*, Open source CFD International conference, Berlin, 2008.